A novel method for the characterization of infiltration airflow using infrared thermography

Diego Tamayo-Alonso[1], Irene Poza-Casado[1], M.Á. Padilla-Marcos[1], Lida Mercado[1], Alberto Meiss[1]

1 GIR Arquitectura & Energía, Dpto. Construcciones Arquitectónicas I.T. y M.M.C.T.E., E.T.S Arquitectura, Universidad de Valladolid ***(Spain)***

**Corresponding author: diego.tamayo@uva.es*
Presenting author: underline First & Last name

ABSTRACT

Controlling air infiltration is crucial to ensure thermal comfort, optimal performance of ventilation systems, and the overall energy efficiency of buildings. The quantification of the overall airtightness of the building envelope, often conducted through pressurization tests, has been widely used. In addition, IR thermography is a valuable complementary tool for identifying and locating air leakage paths.
A methodology to characterize leakage flows based on the bi-dimensional temperature array has been previously developed. This method was proved to be useful, but the total test time is very extensive because several image captures must be performed for to compose a three-dimensional array. This paper presents an optimized methodology where the measuring device is the three-dimensional matrix, obtaining in this way the three-dimensional image of the airflow with a single capture. The objective of this study is to optimize the characterization process of the infiltration airflow using IR thermography, reducing time, and improving its application in practice.
This work opens multiple research lines, for example, the use of the presented methodology coupled with machine learning to estimate the airflow or the characterization of the air distribution of ventilation systems' air inlets.

KEYWORDS

IR thermography, air infiltration, airtightness, leakage paths, leakages.

1 INTRODUCTION

Infrared (IR) Thermography is a technique that enables the measurement of an object's temperature without physical contact (Sarawade & Charniya, 2018). In the construction industry, this technology is increasingly used to identify thermal irregularities, leakages, and humidity issues in building envelopes (Kirimtat & Krejcar, 2018) and assess their impact on energy loss (González-Aguilera et al., 2013). Some researchers combine temperature monitoring with IR cameras to observe how temperatures change throughout the day within structural imperfections. This approach helps avoid errors resulting from interpreting single data points by associating each type of error with an IR representation instead (Fox et al., 2015; Lehmann et al., 2013). Additionally, images of the same defect from both inside and outside of buildings have been studied in order to compare any differences between them (Fox et al., 2016).

The application of IR thermography in detecting and measuring air infiltration has been the subject of previous research and (Barreira et al., 2017; Lerma et al., 2018; Royuela-del-Val et al., 2019). Some authors have identified crack parameters by analysing surface temperatures on the infiltration plane, (Dufour et al., 2009; Liu et al., 2018).

Additionally, IR thermography combined with neural networks has been used to predict airflows based on temperature changes along the air leakage path (Royuela-del-Val et al., 2019). In the same line, Gil-Valverde et al., (2021) proposed a new technique that involved a reduction of the Coanda effect, improving the accuracy and obtaining as a result a three-dimensional characterization of the infiltrating airflows(Gil-Valverde et al., 2021).

This paper presents a step forward based on tests performed in a controlled environment with the objective of obtaining optimized results with a single IR capture. In this way, the possibility of error due to temperature changes during the measuring period is reduced.

2 METHODOLOGY

2.1 Equipment and laboratory experimental set-up

The tests were carried out in the Laboratory of Ventilation located in the School of Architecture of the University of Valladolid. This laboratory has a controlled test chamber with a size of 3.0 m x 4.0 m x 2.5 m (height). Three openings can be configured as inlet or outlet (Figure 1).

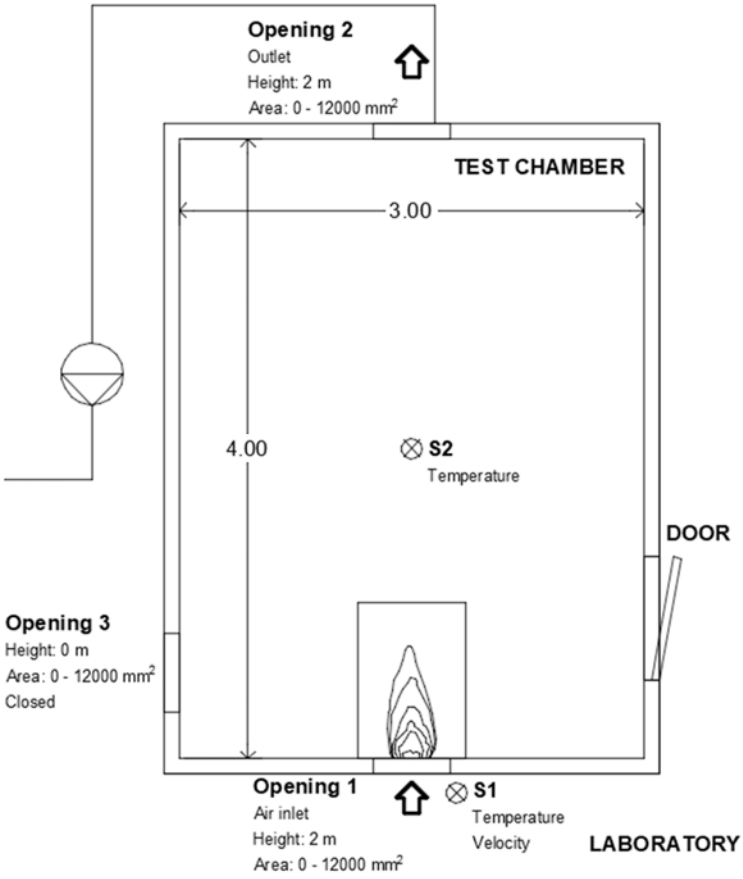

Figure 1. Test chamber configuration floor plan.

The test chamber was set up with the inlet (Opening 1) and exhaust (Opening 2) positioned opposite each other to ensure balanced airflow perpendicular to the wall where the incoming airflow opening was located. To induce air movement, a fan connected to a frequency variator for control purposes was used to create negative pressure inside the chamber. Additionally, the

electric underfloor radiant system with low thermal inertia was activated to maintain approximately 5 ºC temperature difference between the interior (S2) and exterior of the test chamber (S1), thus ensuring accurate boundary conditions. A Lambert radiator was placed under the inlet to mitigate any thermal radiation caused by the heating system.

Three different interchangeable air inlets produced through additive 3D printing were used to ensure precise dimensions of the Opening 1. All inlets shared identical heights but varied in width, resulting in three different air inlet areas (Figure 2).

Figure 2. Incoming airflow openings a) A1. 40 mm x 2.4 mm (96 mm^2) b) A2. 60 mm x 2.4 mm (144 mm^2) c) A3. 80 mm x 2.4 mm (192 mm^2)

The monitorization of the airflow through the test chamber and other parameters as the temperature and velocity of the inlet air was done by a data acquisition system composed of a multisensory data logger, two high-precision temperature sensors (accuracy ±0.1K), a thermal mass flow sensor (accuracy ≤ 3%) and a differential pressure sensor.

The sensible device was a 3D matrix of balls. Each ball works like a temperature sensor, so these balls switched their temperatures by the air temperature. When the temperatures were established, we take a thermal image. The thermal images were captured with an IR camera with a resolution IR of 320 x 240 pixels. These balls were printed with a 3D resin printer. The resin used was black and its emissivity ε=0.95. The 3D matrix had 20 mm of separation in the three dimensions (Figure 3).

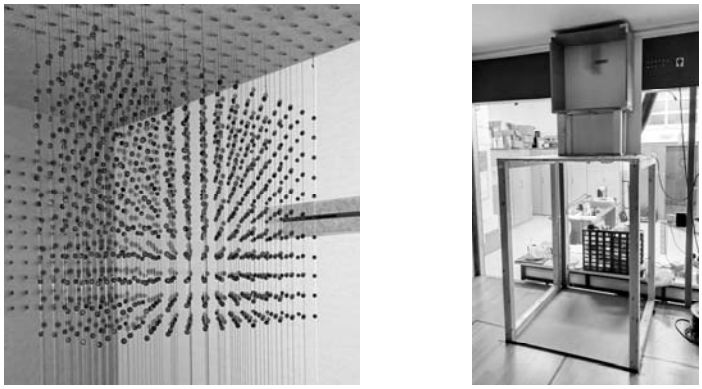

Figure 3. a) 3D Matrix b) Set-up of the experiment

2.2 Experimental design and data processing

During the tests, IR thermal images were captured when the temperatures were stabilized. Unlike other methods (Gil-Valverde et al., 2021) what it needed a lot of thermal images for to

obtain a tridimensional characterization, and therefore it took a long time to stabilize temperatures between each image, now only one thermal image was taken for each setup. This greatly reduces data collection time because we only need waiting the time to stabilized the temperatures one time. Also, all the points were measured at the same time, which avoided the need to adjust temperatures between samples.

The location of the camera was essential for the automation of temperature extraction. Therefore, the camera position, as well as its setup, remained unchanged to guarantee the visualization of the points in the central axis of the opening. Only one-half of the airflow was studied assuming a symmetrical pattern (Gil-Valverde et al., 2021).

The tests were performed considering three different flow rates (Q1, Q2, and Q3) per opening (A1, A2, and A3). The following data were also registered for each IR thermal image: indoor temperature (T_{int}), outdoor temperature (T_{ext}), temperature gradient (ΔT), air flow rate (Q), pressure differential (ΔP), medium air velocity at the opening, inferred from the airflow rate (V), and the opening dimensions, according to the Continuity Law of Fluids (Table 1).

Table 1: Data registered during the tests

	A1-Q1	A1-Q2	A1-Q3	A2-Q1	A2-Q2	A2-Q3	A3-Q1	A3-Q2	A3-Q3
Q (m^3/h)	1.4	2.4	3.8	2.2	3.1	5.1	2.7	4.7	5.7
ΔP (Pa)	1.6	10.8	36.00	1.28	4.8	35.3	0.9	10.4	34.8
T_{int} (ºC)	26.1	26.3	26.0	26.0	25.3	25.4	24.9	24.6	24.7
T_{ext} (ºC)	20.9	21.0	20.9	20.5	20.3	20.2	19.7	19.6	19.5
ΔT (ºC)	5.2	5.3	5.1	5.5	5.0	5.2	5.2	5.0	5.2
V (m/s)	3.9	7.1	10.9	4.2	6.0	9.9	3.9	6.8	8.2

The first step was to identify the points to be extracted from the image by creating a mapping of the "pixels" and the points of one-half of the 3D matrix. The viewpoint is very important to view most of the balls. In this set, only 3.7% of the balls were hidden, moreover, these hidden balls belonged, in this case, to areas away from the airflow, so they did not interfere with the measurement. The second step involved the processing of all the images with MATLAB. The temperature values of the previously selected points were extracted. After that, the 3D representation of the whole matrix and every plan section in the edges X, Y, and Z is obtained (Figure 5).

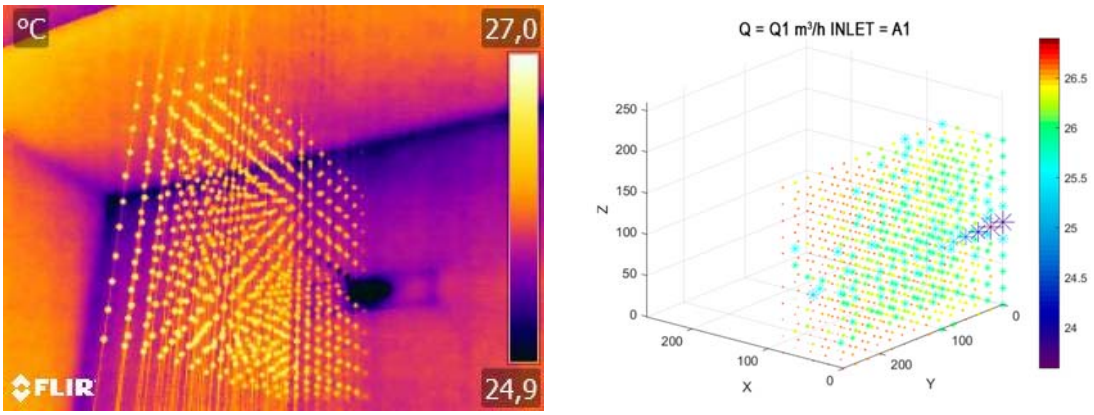

Figure 4. Images of the airflow A1-Q1. a) Thermal image b) 3D representation of half the airflow

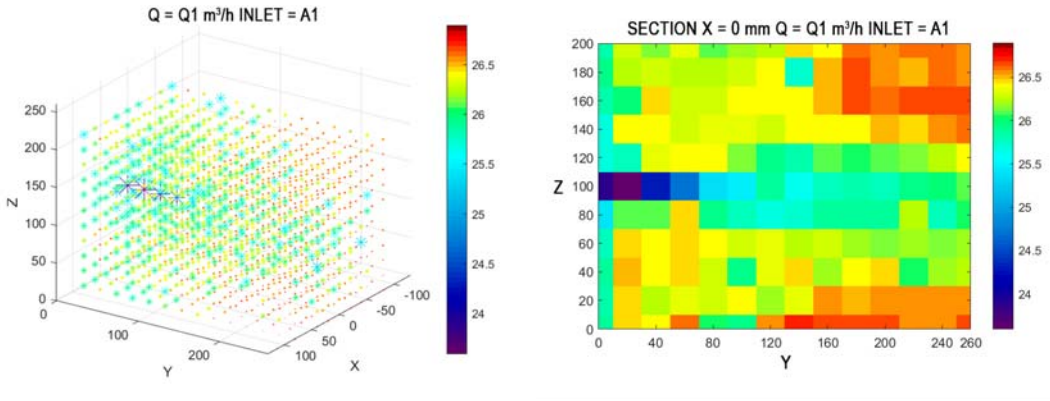

Figure 5. Images of the airflow A1-Q1. a) Complete 3D representation b) Measurement of plane ZY at 0 mm from the opening's axis

3 RESULTS

The following graphs were created by combining the different openings and airflows resulting from only one IR thermal image, along with the post-processing of the captures (see Figure 6). The variation in the airflow path can be observed based on the parameters.

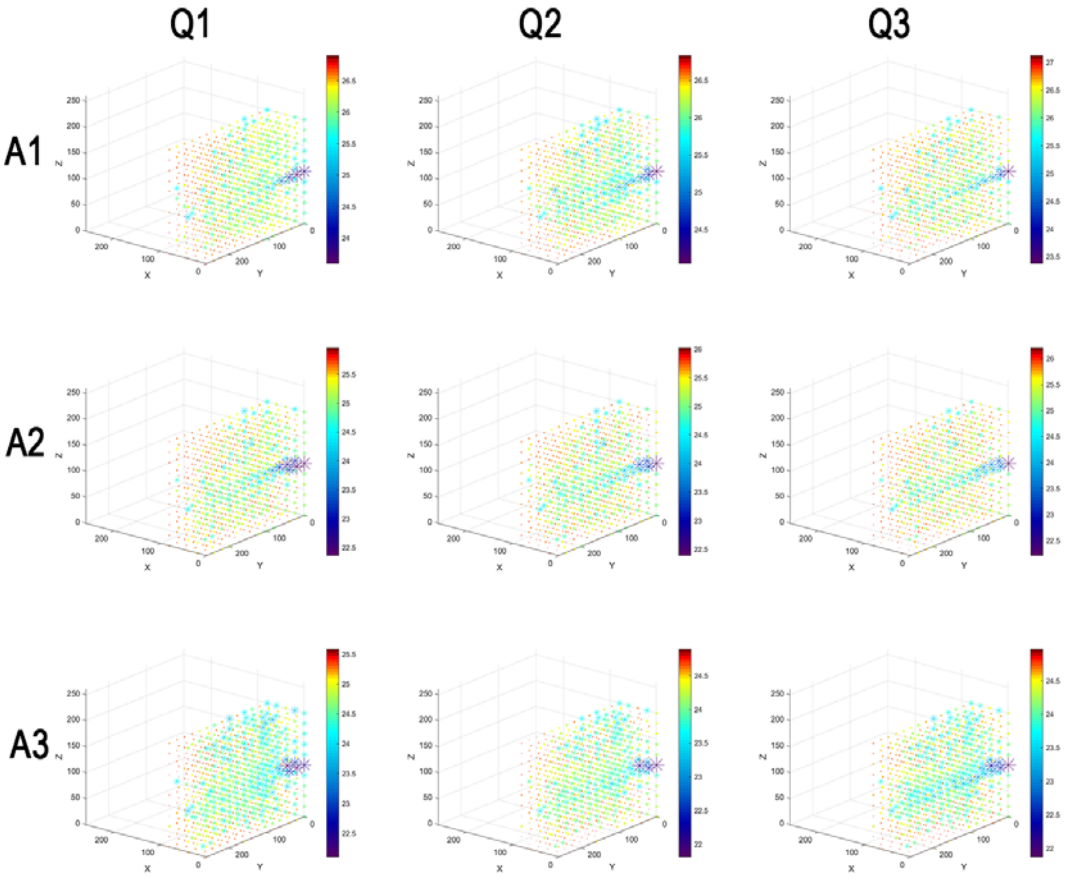

Figure 6. Three-dimensional representation of one-half of the airflow a) A1-Q1 b) A1-Q2 c) A1-Q3 d) A2-Q1 e) A2-Q2 f) A2-Q3 g) A3-Q1 h) A3-Q2 i) A3-Q3

It can be observed how the airflow changes with the size of the inlet and the airflow rate. As an example, the results obtained for the measurement plane on the inlet axis can be seen in Figure 7. We can see how at an opening, as the flow rate increases, the flow appears to stretch due to the increased velocity of the air. If we look at the lower flow rate (Q1) it appears that the air has a slight tendency to go down, due to the lower velocity, and that being cold air, due to the lower density, it tends to go down. At the other flow rates this phenomenon will also occur, but as the air exits at a higher velocity, this occurs outside the measurement area.

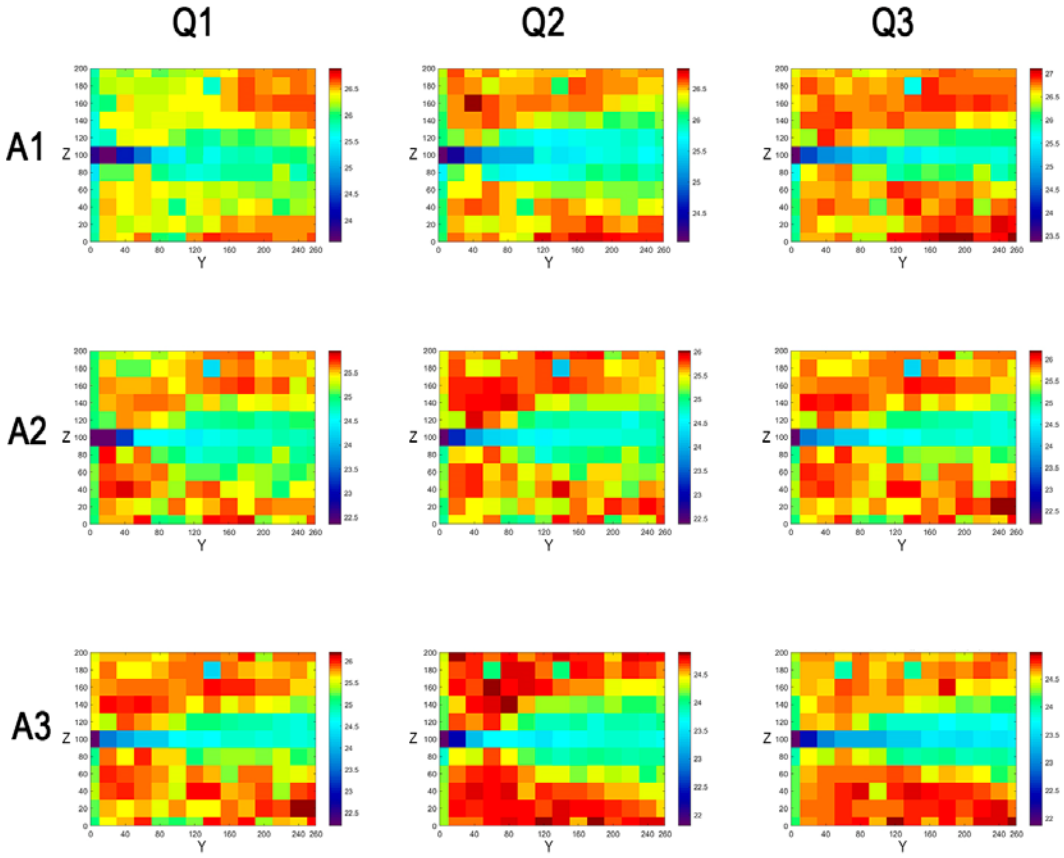

Figure 7. Measurement plane ZY at 0 mm from the opening's axis a) A1-Q1 b) A1-Q2 c) A1-Q3 d) A2-Q1 e) A2-Q2 f) A2-Q3 g) A3-Q1 h) A3-Q2 i) A3-Q3

4 CONCLUSIONS

This paper presents an optimized technique for the characterization of airflows through controlled air inlets. In contrast with previous methods, which required a lot of data collection time, the advantage is that only one IR thermal image is needed for each airflow condition, and that makes it possible to transfer the method to a real situation in a building. Also, the need for a single thermal image avoids uncertainties regarding pressure and temperature changes during the measurement or even camera location variation due to limited battery life.

This method to characterize airflows opens new possibilities about several research lines such as the quantification of leakages, the in-situ evaluation of the operating regime of ventilation grids, or the validation of CFD systems.

5 REFERENCES

Barreira, E., Almeida, R. M. S. F., & Moreira, M. (2017). An infrared thermography passive approach to assess the effect of leakage points in buildings. *Energy and Buildings*, *140*, 224–235. https://doi.org/10.1016/j.enbuild.2017.02.009

Dufour, M. B., Derome, D., & Zmeureanu, R. (2009). Analysis of thermograms for the estimation of dimensions of cracks in building envelope. *Infrared Physics and Technology*, *52*(2–3), 70–78. https://doi.org/10.1016/j.infrared.2009.01.004

Fox, M., Coley, D., Goodhew, S., & De Wilde, P. (2015). Time-lapse thermography for building defect detection. *Energy and Buildings*, *92*, 95–106. https://doi.org/10.1016/j.enbuild.2015.01.021

Fox, M., Goodhew, S., & De Wilde, P. (2016). Building defect detection: External versus internal thermography. *Building and Environment*, *105*, 317–331. https://doi.org/10.1016/j.buildenv.2016.06.011

Gil-Valverde, R., Tamayo-Alonso, D., Royuela-del-Val, A., Poza-Casado, I., Meiss, A., & Padilla-Marcos, M. Á. (2021). Three-dimensional characterization of air infiltration using infrared thermography. *Energy and Buildings*, *233*, 110656. https://doi.org/10.1016/J.ENBUILD.2020.110656

González-Aguilera, D., Lagüela, S., Rodríguez-Gonzálvez, P., & Hernández-López, D. (2013). Image-based thermographic modeling for assessing energy efficiency of buildings façades. In *Energy and Buildings* (Vol. 65, pp. 29–36). https://doi.org/10.1016/j.enbuild.2013.05.040

Kirimtat, A., & Krejcar, O. (2018). A review of infrared thermography for the investigation of building envelopes: Advances and prospects. *Energy and Buildings*, *176*, 390–406. https://doi.org/10.1016/j.enbuild.2018.07.052

Lehmann, B., Ghazi Wakili, K., Frank, T., Vera Collado, B., & Tanner, C. (2013). Effects of individual climatic parameters on the infrared thermography of buildings. *Applied Energy*, *110*, 29–43. https://doi.org/10.1016/j.apenergy.2013.03.066

Lerma, C., Barreira, E., & Almeida, R. M. S. F. (2018). A discussion concerning active infrared thermography in the evaluation of buildings air infiltration. *Energy and Buildings*, *168*, 56–66. https://doi.org/10.1016/j.enbuild.2018.02.050

Liu, W., Zhao, X., & Chen, Q. (2018). A novel method for measuring air infiltration rate in buildings. In *Energy and Buildings* (Vol. 168, pp. 309–318). https://doi.org/10.1016/j.enbuild.2018.03.035

Royuela-del-Val, A., Padilla-Marcos, M. Á., Meiss, A., Casaseca-de-la-Higuera, P., & Feijó-Muñoz, J. (2019). Air infiltration monitoring using thermography and neural networks. *Energy and Buildings*, *191*, 187–199. https://doi.org/10.1016/J.ENBUILD.2019.03.019

Sarawade, A. A., & Charniya, N. N. (2018). Infrared Thermography and its Applications: A Review. *2018 3rd International Conference on Communication and Electronics Systems (ICCES)*, *Icces*, 280–285. https://doi.org/10.1109/CESYS.2018.8723875